Computers and Concrete, *Vol. 26, No. 3* (*2020*) *227-237*
DOI: https://doi.org/10.12989/cac.2020.26.3.227

Determination of plastic concrete behavior at different strain rates to determine Cowper-Symonds constant for numerical modeling

Reza Nateghi[a], Kamran Goshtasbi* and Hamid Reza Nejati[b]

Faculty of Engineering, Tarbiat Modares University, Jalal AleAhmad Nasr, Tehran, P.O. Box: 14115-111, Iran

(*Received July 20, 2019, Revised January 8, 2020, Accepted August 7, 2020*)

Abstract. Strain rate investigations are needed to calibrate strain-rate-dependent material models and numerical codes. An appropriate material model, which considers the rate effects, need to be used for proper numerical modeling. The plastic concrete cut-off wall is a special underground structure that acts as a barrier to stop or reduce the groundwater flow. These structures might be subjected to different dynamic loads, especially earthquake. Deformability of a structure subjected to dynamic loads is a principal issue which need to be undertaken during the design phase of these structures. The characterization of plastic concrete behavior under different strain rates is essential for proper designing of cut-off walls subjected to dynamic loads. The Cowper-Symonds model, as one of the most commonly applied material models, complies well with the behavior of a plastic concretes in low to moderate strain rates and will be useful in explicit dynamics simulations. This paper aims to present the results of an experimental study on mechanical responses of one of the most useful types of plastic concrete and Cowper-Symonds constant determination procedures in a wide range of strain rate from 0.0005 to 107 (1/s). For this purpose, SHPB, uniaxial, and triaxial compression tests were done on plastic concrete samples. Based on the results of quasi-static and dynamic tests, the dynamic increase factors (DIF) of this material in different strain rates and stress state conditions were determined for calibration of the Cowper - Symonds material models.

Keywords: Cowper-Symonds model; plastic concrete; dynamic test; DIF; strain rate

1. Introduction

The dynamic mechanical behavior of a material is significantly affected by the loading rate (Dharan and Hauser 1970). Dynamic strength enhancement is critical for the calibration of numerical models that are often employed in analysis and design. In 1957, Cowper and Symonds introduced their constitutive equation to characterize the effect of strain rate on material properties (Jones 1989). Their model was formulated based on the dynamic lower yield stress test data obtained from various materials at different strain rates (Marais and Tait 2004). Many investigations have been carried out on this effect over the last century, and similar models were proposed by some researchers, like Cook, Johnson, Zerilli, Armstrong, etc. (Al Salahi and Othman 2016). It is clear that concrete is a strain-rate-sensitive material; it exhibits different characteristics, namely, an increase in strength with increasing strain rates (Ritchie *et al*. 2017). Abrams (1917) was the first researcher who noted, that the behavior of concrete is related to strain rates (Bischoff and Perry 1991). According to the literature (Sfer *et al*. 2002, Zhao and Lok 2005, Brara and Klepaczko 2006, Riisgaard *et al*. 2007, Zhang *et al*. 2008, Cusatis 2011, Pajak 2011, Li *et al*. 2012, Chen *et al*. 2013, Pandey 2013, Kai *et al*. 2016, Sakai *et al*. 2016, Rukhaiyar *et al*. 2017, Guo *et al*. 2017, He and Ding 2019), dynamic behavior of regular concrete and other cement-based materials used in modern construction was studied within a wide range of researches. Furthermore, a literature survey shows that the dynamic strength of plastic concrete has not yet been studied, and this paper is the product of primary research in this field. Cut-off wall structures may be subjected to dynamic loads such as blast waves, earthquake or roller compact waves, during construction and after operation that can produce low (0.001-1 s^{-1}) to intermediate (1 to 100 s^{-1}) strain rates which significantly alters the plastic concrete behavior. Due to the lack of data on the plastic concrete behavior under different strain rates, an experimental program was run at the Tarbiat Modares rock mechanic laboratory and impact laboratory of Bu Ali Sina University on one of the most useful types of the plastic concrete mixture at low to moderate strain rates. The framework of this study is based on experimental results from laboratory tests and a presentation of the statistical relationships between plastic concrete strength parameters under different stress conditions and strain rates. Fig. 1 shows the overview of laboratory tests and results for each section.

These data were used to determination the Cowper-Symonds parameters. The results can now be used to determine the strength increase of plastic concrete structures subject to a wide range of impulses, to create the input data required for numerical analysis.

*Corresponding author, Professor
E-mail: goshtasb@modares.ac.ir
[a]Ph.D. Candidate
E-mail: r.nateghi@modares.ac.ir
[b]Associate Professor
E-mail: h.nejati@modares.ac.ir

http://www.techno-press.org/?journal=cac&subpage=8
ISSN: 1598-8198 (Print), 1598-818X (Online)

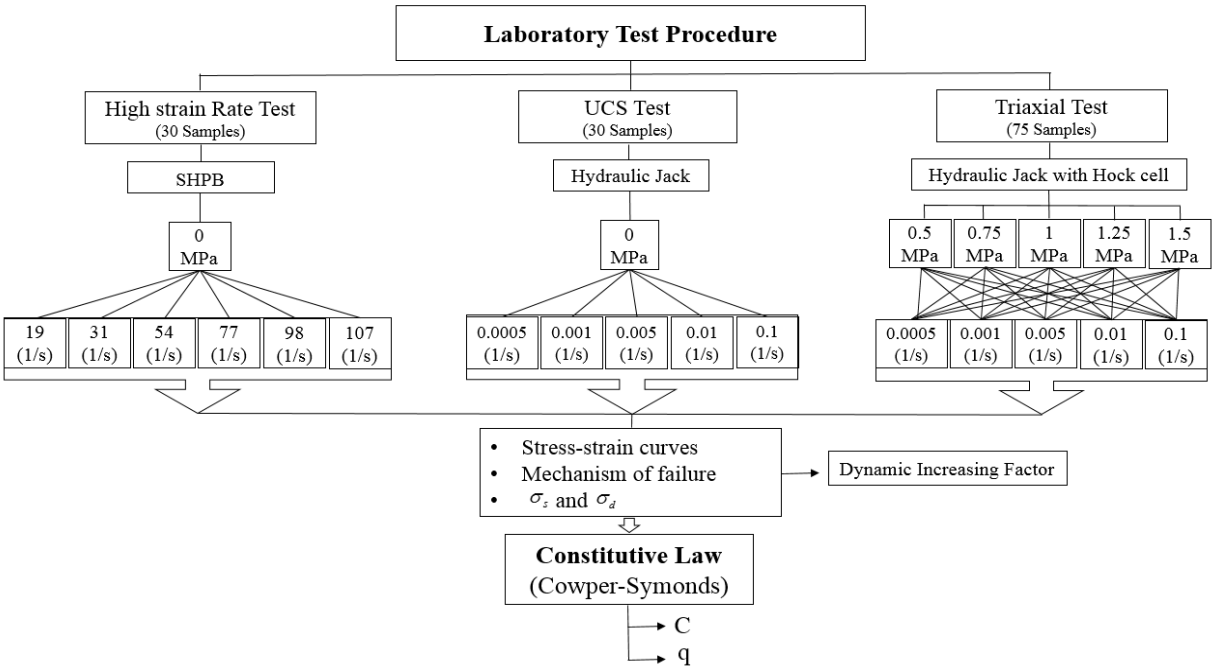

Fig. 1 Overview flowchart of laboratory tests and results

2. Strain rate by dynamic waves

Some researchers have tried to correlate induced stress developed by dynamic waves with the strength of the structure's materials (Ngo *et al*. 2007, Gad *et al*. 2005). The strain induced by the dynamic waves in soil and rock can be calculated using Eq. (1)

$$\varepsilon = \frac{\partial u}{\partial x} = \frac{\partial u}{\partial t}\frac{\partial t}{\partial x} = v.\frac{1}{c_p} \tag{1}$$

Where (u) is the particle displacement, (v) is the particle velocity, (t) is the time, (x) is the travelling distance of the wavefront, and (Cp) is the *P*-wave velocity.

The acceleration is

$$a = \frac{\partial v}{\partial t} \tag{2}$$

Therefore, the strain rate is

$$\dot{\varepsilon} = \frac{\partial v}{\partial x} = \frac{\partial v}{\partial t}\frac{\partial t}{\partial x} = a.\frac{1}{c_p} \tag{3}$$

In this equation, ($\dot{\varepsilon}$) is the strain rate and (a) is the particle acceleration. According to Eq. (3), the strain rate induced by dynamic loads is corresponding to the maximum particle acceleration (PGA) and *P*-wave velocity in a medium. Fig. 2 shows a schematic range of the strain rate from different activities. Since the cut-off wall may be exposed to the blasting waves from construction activities, earthquakes, and vibration from rollers, this study focuses on the behavior of plastic concrete in these ranges. Accordingly, the majority of the recent researches into the strain rate behavior of the plastic concrete has been conducted in the range of 0.0005 to 107 that covers the whole spectrum of possible strain rates that a cut-off wall may be subjected to them. This information can help better understand the behavior of the plastic concrete in order to design the structures using this material in construction and to increase the accuracy of numerical models.

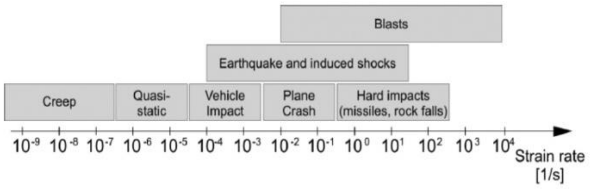

Fig. 2 Ranges of the strain rate from different activities

3. Plastic concrete

Plastic concrete is a newly developed watertight material with low permeability. It comprises a mixture of cement, water, aggregate, and bentonite. It has a low modulus of deformation. Therefore, it can favorably adapt the deformation of surrounding soils and will allow the deformation of the wall and ground without separation. Furthermore, it has excellent ductility after reaching failure compared with regular concrete (Fig. 3) (Nateghi *et al*. 2020).

Plastic concrete is used in the construction of seepage cut-off walls in dams. Characteristics of the cut-off wall material should be assigned in a way that ensures the required impermeability, deformability and strength. The International Committee of Large Dams (ICOLD) indicated that a material, having a deformability modulus of 4 to 5 times greater than the surrounding area, would be suitable (ICOLD Bulletin No. 51 1985). Table 1 shows the mixed design and pertinent parameters of plastic concrete used as the cut-off wall materials in the Gotvand dam project. The

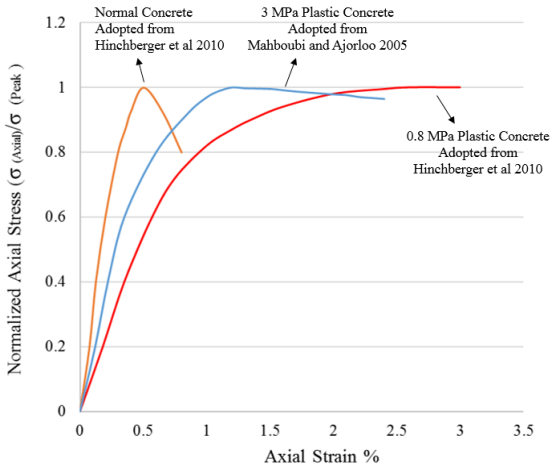

Fig. 3 Stress-strain response of regular concrete compared with plastic concrete

Table 1 The plastic concrete mixture used in the Gotvand cut-off wall

Mix	W/C	B/C	Cement (Kg)	Bentonite (Kg)	Water (Kg)	Sand (Kg)	Coarse aggregate (Kg)
PC30	1.65	0.15	200	30	330	702	859

cement used in the mixed design was a sulfate resistant cement (type V) from Abyek Cement Company, and the bentonite was acquired from Salafchegan. In order to have very low permeability, the bentonite was mixed with 90% of water prior to the sample preparation. This Mix was designed to reach a compressive strength of about 3MPa and permeability of about 10^{-8} to 10^{-9} (m/s). The shear strength parameters of this mixture (C and φ), resulted from Mohr envelope in the triaxial test, is about 40° and 0.08 (MPa).

4. Experimental procedure

4.1 UCS and triaxial test

Herein, 30 samples of plastic concrete have been prepared for unconfined compression tests and 75 samples for triaxial compression tests. Specimens were prepared in 5.2 cm in diameter and 10.5 cm in height and were kept underwater. The ends of each sample were grounded to be flat and parallel to each other. The sonic velocity of each sample was measured by ultrasonic test before loading. From the results of these tests, the P-wave velocity in this medium is about 2850 (m/s). The low strain rate tests in UCS and triaxial tests were performed utilizing a hydraulic servo-controlled machine in rock mechanic laboratory of Tarbiat Modares University. Tests were carried out in the displacement control mode. In triaxial tests, a Hock cell was used to exert the confining pressure. The cylindrical samples were placed into a chamber within a confining membrane. The cell was placed in a loading frame, after applying a little confining pressure to hold the samples in place. The triaxial tests may then be run after adjustment of the confining pressure to the required values. Lateral

Fig. 4 Some of the apparatuses that were used for triaxial tests

pressure was generated through an adjustable spring-type deadweight accumulator system connected to a pump and an oil interchange plastic pipe. Fig. 4 shows some of the apparatuses used for triaxial tests.

Axial displacement was monitored by a linear variable differential transformer (LVDT). As seen in Fig. 5 this device was located between the jaws. UCS and triaxial compression tests were performed at five different strain rates of 0.0005, 0.001, 0.005, 0.01, and 0.1 (1/s) and five confining pressure of 500, 750, 1000, 1250, and 1500 (KPa) in triaxial tests. According to the recommendations of American Society for Testing and Materials (ASTM D2166) and (ASTM-D2850 1987) about the UCS and triaxial tests, a strain rate of 0.0005 (1/s) has been selected for specimens with 10.5 cm height to satisfy the static condition requirements throughout the experiments. This should be noted that in each strain rate in UCS, and triaxial tests, loading was performed on 6, and 3 of samples, respectively. The mean values of the results in each strain rate were used for calculation of DIF.

4.2 SHPB test

The intermediate strain rate tests were carried out using a Split Hopkinson Pressure Bar at six different strain rates (19, 31, 54, 77, 98, and 107 (1/s)). The equipment selected for this impact compression tests was a SHPB test device in impact laboratory of Bu Ali Sina University. The equipment selected for this impact compression test is a 25.4 mm diameter SHPB test device. The striker, an incident rod, and transmission bar were all made from stainless steel; their lengths were 200 mm, 1530 mm, and 1200 mm, respectively. The rods density is equal to 7850 (Kg/m^3), and the wave velocity in bars is equal to 5100 (m/s). The strain gauges were installed in the middle of the transmission and incident bars. A view of the apparatus is shown in Fig. 7. The 30 samples that were used in SHPB test had a cylindrical shape with the length and diameter of 50 and 25 (mm), respectively. These dimensions choose based on the suggestion of Davies and Hunter. They suggested that the optimum aspect ratio (L/D) be $\frac{L}{D}=\sqrt{\frac{3}{4}\upsilon}$ (where (υ) is the Poisson's ratio of the specimen material). In most cases, this condition yields L/D=0.5. In the experiments conducted here, all samples have the same aspect ratios equal to 0.5. in SHPB test the striker bar, propelled by a pressurized gas,

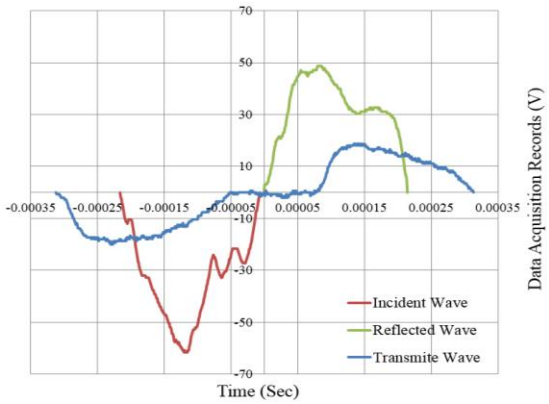

Fig. 5 A sample of the incident, reflected, and transmitted signals

impacts against the input bar. A compressive stress pulse is generated in the striker and input bar. It then impinges on the specimen between the input and output bars. A part of the incident pulse is reflected back into the input bar from the input bar/specimen interface, and a part of it is transmitted through the specimen into the output bar. A strain gauge is placed on the input bar and another on the output bar. The strain gages output signals are recorded on a digital oscilloscope. Fig. 5 shows the signals recorded from the strain gauges mounted on the input and output bars during an experiment.

These strain measurements are used to determine the time histories of the stress, strain and strain rate in the specimen during deformation. Specifically, the stress (σ) and strain rate ($\dot{\varepsilon}$) histories are as Eqs. (4) -(5) respectively (Lindholm 1964).

$$\sigma = \frac{A_0}{A} E_0 \varepsilon_T(t) \tag{4}$$

$$\dot{\varepsilon} = -\frac{2c_0}{L} \varepsilon_R(t) \tag{5}$$

The expression for the strain rate in Eq. (5) may be integrated with respect to time to give the strain (ε), i.e.

$$\varepsilon = -\frac{2c_0}{L} \int_0^t \varepsilon_R(t) dt \tag{6}$$

In these equations (E_0), (A_0), and (c_0) denote Young's modulus, cross-sectional area and longitudinal wave speed of the bars, and (A) and (L) are the cross-sectional area and length of the specimen, respectively. In these equations (ε_T) and (ε_R) denote the amplitudes of the transmitted and reflected strain pulses, respectively (Yiben *et al*. 2019). Five samples were tested in constant gas pressure, and the mean values were proposed as the stress, strain, and strain rate values.

5. Mechanism of failure

Fig. 6 illustrates the failure mechanism of the plastic concrete samples. As can be seen in this figure, in USC tests, at static and quasi-static strain rates, failure occurs

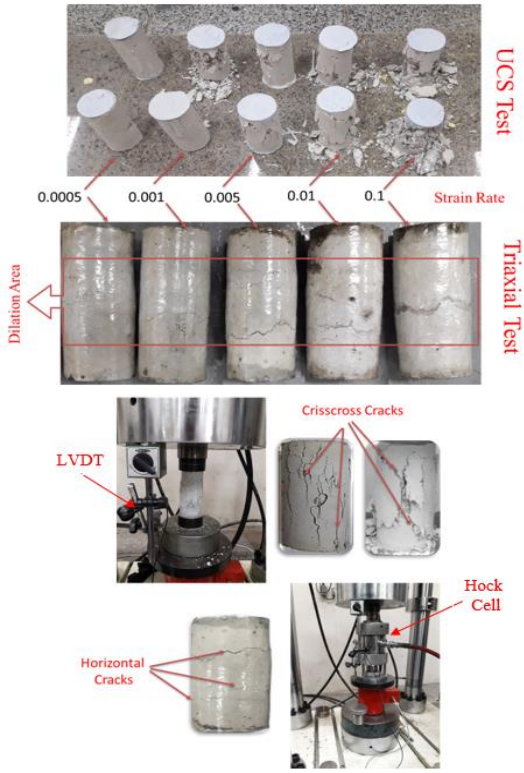

Fig. 6 Comparison of the failure mechanism in UCS and triaxial compression tests

Fig. 7 SHPB device for intermediate strain rate tests and fractured samples

with the propagation of several distributed vertical and inclined cracks.

The overall shape of plastic concrete samples remains unchanged but with many visual crisscross cracks on its surface. At higher strain rates, the mechanism of failure consists of the spreading of angular cracks in the samples. This causes the samples to split into several pieces or even collapse under higher strain rates. In triaxial tests, the mechanism of failure consists of lateral dilation mainly in the middle section of the samples and the spread of horizontal cracks which also cause the samples to split into several pieces. This mechanism is the same in different strain rates.

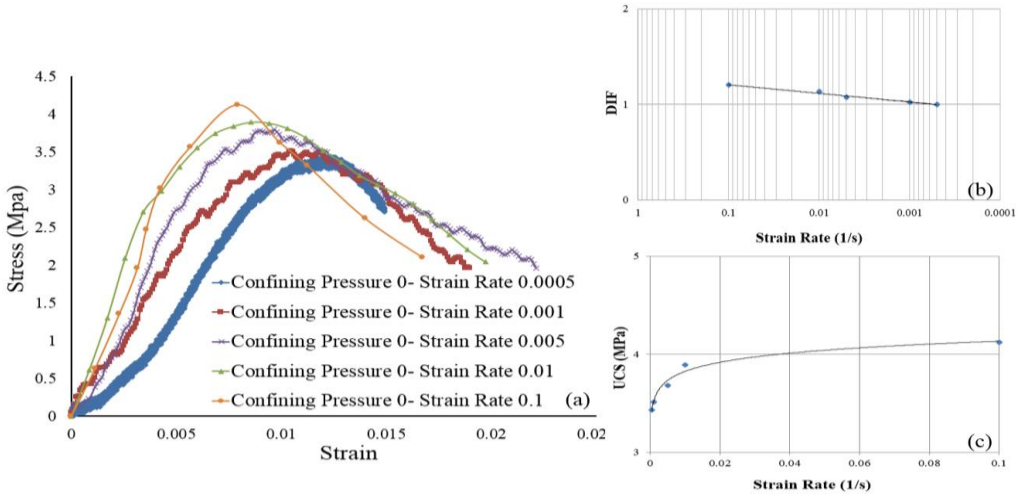

(a) Stress-strain curves (b) DIF-strain rate curve (c) UCS-strain rate curve

Fig. 8 Stress-strain curves and changes in compressive strength and DIF in UCS tests

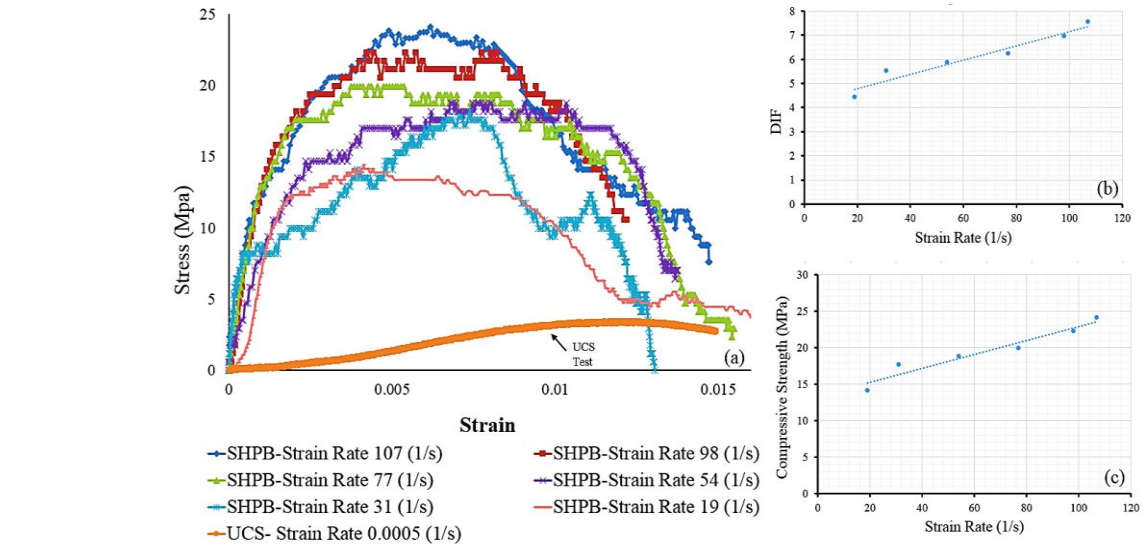

(a) Stress-strain curves (UCS&SHPB) (b) DIF-strain rate curve (c) UCS-strain rate curve

Fig. 9 Stress-strain curves and changes in compressive strength and the DIF in the SHPB test

Fig. 7 shows the apparatus used for SHPB tests and status of samples after loading. As seen in this figure, at strain rates of loading (19-107 1/s), the mechanism of failure consists of the spreading of longitudinal cracks in the samples that causes the samples to split into several prismatic pieces.

6. Results and discussion

The results, in terms of stress versus strain curves and the values of DIF and strength of samples in compressive UCS, triaxial, and SHPB tests at different strain rates, are shown in Figs. 8-10. DIF is the ratio of the dynamic strength of the samples in the dynamic states of loading to the strength of the samples in the static state condition. Such a definition of DIF is optimal because it normalizes different dynamic strengths due to different strain rates, specimen scales, and shapes (Pajak 2011). Fig. 8 shows the stress-strain curves (Fig. 8(a)) and the relationship between the DIF (Fig. 8(b)) and the uniaxial compressive strength (Fig. 8(c)) versus the log of the strain rates. It shows that the uniaxial compressive strength of plastic concrete samples increases continuously with increasing the strain rate. An increase of 20% was observed in DIF when the strain rate was increased from 0.0005 to 0.1 (1/s). An increase in the uniaxial compressive strength of normal concrete with increasing loading rate has been reported by many other researchers (Tay 2009, Kim *et al*. 2010, Weerheijm and Van Doormaal 2007). This phenomenon is the results of a reduction in the possibility of crack propagation around the aggregates. It was noted that the relationship between the DIF and UCS versus the strain rate could be described by the Eqs. (7) and (8).

$$DIF = 0.039\ln(\dot{\varepsilon}) + 1.295 \tag{7}$$

$$\sigma_d = 0.134\ln(\dot{\varepsilon}) + 4.442 \tag{8}$$

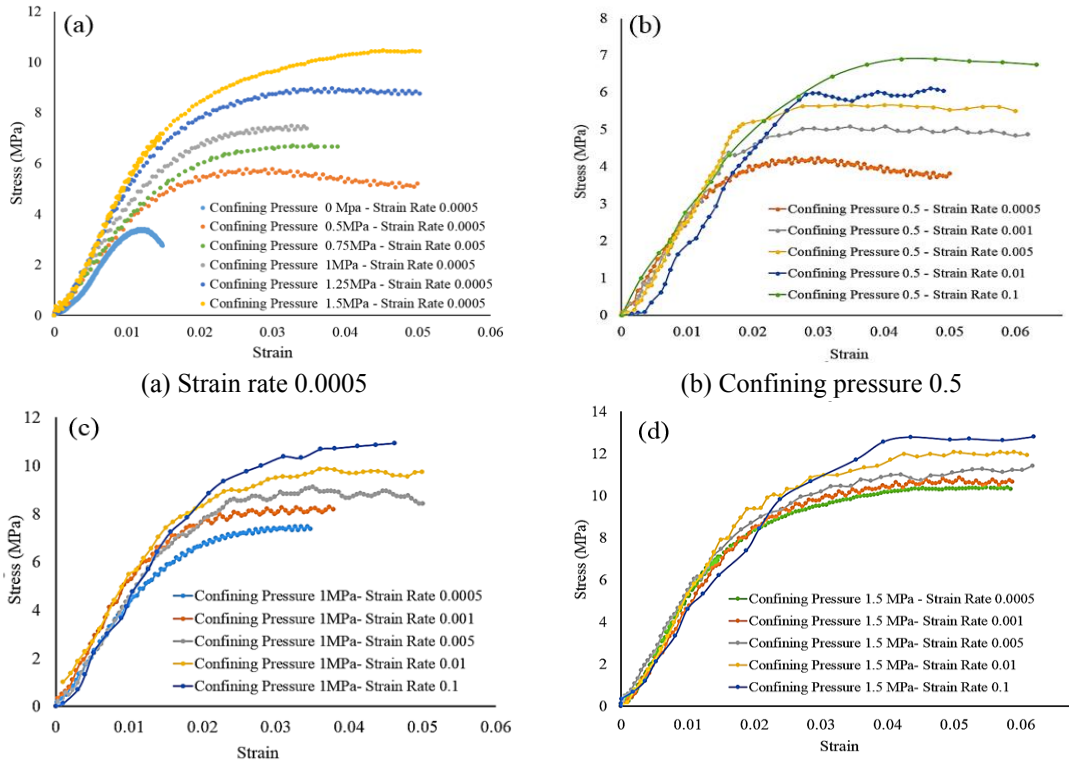

(a) Strain rate 0.0005 (b) Confining pressure 0.5

(c) Confining pressure 1 (d) Confining pressure 1.5

Fig. 10 The stress-strain curves of plastic concrete in different confining pressures and strain rates

In these equations, (σ_d) is the peak of quasi-static and dynamic uniaxial compression strength (MPa) and ($\dot{\varepsilon}$) (1/s) is the strain rate that ranges from 0.0005 to 0.1 (1/s). Fig. 9 shows typical dynamic stress-strain curves and effects of strain rate on increasing the strength of plastic concrete, in the SHPB test. The strain rate is not constant during the tests; even if the gas pressure is kept constant.

An average of maximum strain rate is calculated and used for each step of loading. The stress-strain history computed, according to Eqs. (4) and (6). The history of stress and strain combine to yield the stress-strain curves shown in Fig. 9(a). Experimental results, with a strain ratio in the mentioned range, indicates that most of the stress-strain curves usually rise in line with positive slope in the first part, the curve is rather horizontal in the middle, then the strain increases continuously with the stress and the ability of withstanding load decreases, even when the stress decreases to zero. The approximate horizontal line in the middle of the curve indicates the plastic characteristic of concrete after being impacted. The results are presented as DIF (Fig. 9(b)) and compressive strength (Fig. 9(c)) versus strain rate. DIF is the ratio of the dynamic strength to strength of plastic concrete under static loading. The trend of the results shows that compressive strength increases with increasing the strain rate. The values of the DIF factor are in the range of 4.42 to about 7.03. In the SHPB test, the best-fitted line between DIF versus the strain rate is in the form of the Eq. (9)

$$DIF = 0.0297(\dot{\varepsilon}) + 4.184 \tag{9}$$

This equation can be used to predict DIF for a value of strain rate (1/s), or find the settings for strain rate that corresponds to a desired value or range of values for DIF. The relationship between the dynamic compressive strength and the loading rate from SHPB test could be described by Eq. (10):

$$\sigma_d = 0.09519(\dot{\varepsilon}) + 13.36 \tag{10}$$

To compare the effect of strain rate on the strain of plastic concrete in unconfined tests, the stress-strain curve of this material in static state of loading in UCS test was added next to the results of stress-strain history of samples under SHPB tests in Fig. 9(a). As shown in this figure, with increasing the strain rate in SHPB test, the strength of the samples was increased and their strain was decreased obviously in yield point. The changes mentioned in these two parameters have significant effects on the elastic modulus of plastic concrete. The results of enhancement in DIF, in low and moderate strain rate, in UCS and SHPB tests comply well with the researches done on other cemented- based materials (Pajak 2011, Sheng *et al*. 2013). Fig. 10(a)-(d) shows the stress-strain responses of some specimens in different confining pressures when increasing the strain rate from 0.0005 to 0.1 (1/s) in the triaxial tests. Fig. 10(a) illustrates the stress-strain behavior of some specimens in a constant strain rate while the confining pressure increases from 0.5 to 1.5 (MPa). It is evident that in a constant strain rate, increasing the confining pressure will increase the strength of the specimens. Furthermore, the plastic concrete behavior tends to be brittle at zero or low values of confining pressure. Also, a well-defined peak is observed in the stress-strain curves, and the samples have

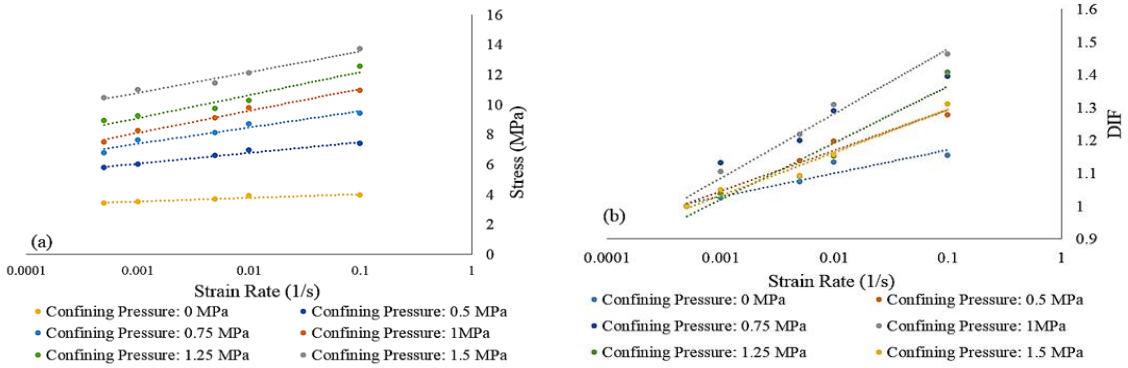

(a) Stress-strain rate curves (b) DIF-strain rate curves

Fig. 11 Changes in the compressive strength and DIF at different strain rates and confining pressures

subsequent softening behavior, whereas at the high confining pressures the behavior of plastic concrete will be more ductile. These results comply well with the other similar researches in this field (Sfer *et al*. 2002, Naderi 2005, Mahboubi and Ajorloo 2005, Pashang and Hosseini 2012). Fig. 10(b)-(d) illustrates the stress-strain behavior of some specimens in constant confining pressure, while the strain rates increase from 0.0005 to 0.1 (1/s). It is evident that in constant confining pressure, increasing the strain rate will increase the strength of the specimens. It can be concluded that increasing the strain rate and confining pressure, increases the strength of the specimens.

Fig. 11(a) shows the relationship between the triaxle compressive strength and strain rate.

Generally, obtained results show that the compressive strength increases with increasing the strain rate. In addition, in triaxial tests, the trend of strength enhancement is much steeper than UCS tests. Furthermore, the slope of the regression lines increases slightly with increasing the confining pressure. An enhancement of 28%-45% was observed in strength when the strain rate and confining pressure were increased from 0.0005 to 0.1 (1/s) and 0.5 to 1.5 (MPa), respectively. While the results of UCS tests show a slight increase in concrete compressive strength with increasing strain rate up to 20%. Fig. 11(b) shows the effect of strain rate on DIF in different confining pressures and strain rates. DIF is defined as the ratio of the dynamic strength to the strength of plastic concrete in the static state loading (0.0005 (1/s)) in the UCS test. As for the compressive strength, the DIF depends on the confining pressure as well as the strain rate in a way that the DIF increases with increasing the confining pressure or strain rate. For the mentioned specimens, DIF obtained in triaxial compression tests might increase up to 48%, depending on confining pressure and strain rate.

7. Constitutive law (Cowper-Symonds)

Over the years, several models have been proposed that relate the dynamic strength to the strain rate. In 1957, Cowper and Symonds developed a constitutive model that defined DIF as a function of strain rate, using a power-law relationship (Yu *et al*. 2013). It is shown in Eq. (11)

$$DIF = \frac{f_{dy}}{f_y} = 1 + \left(\frac{\dot{\varepsilon}}{C}\right)^{1/q} \tag{11}$$

where C and q are Cowper-Symonds fitting parameters. Since the model was proposed, numerous researchers have suggested new Cowper-Symonds parameters for various materials. Cowper - Symonds model, as a plastic-kinematic hardening model, is suited to model strain rate dependent materials. It is often used in finite element analysis to quantify the strain rate dependence of materials subjected to dynamic loads (Krishnappa *et al*. 2013, Zhang *et al*. 2015, Ngo *et al*. 2015). This should be noted that the Cowper-Symonds model is an empirical equation that is based on observations. The procedure to evaluate the parameters of the Cowper-Symonds elastic-plastic material model can be explained in simple words as follows. Once the dynamic stress-strain data for a specific elastic-plastic material is available, we can plot the ratio of the dynamic yield stress (sigma-sub-d.) to the initial static yield stress (sigma-sub-s) versus the strain rate. Rewriting the Eq. (11) results in Eq. (12)

$$\frac{\sigma_d - \sigma_s}{\sigma_s} = \left[\left(\frac{\dot{\varepsilon}}{C}\right)^{\frac{1}{P}}\right] \tag{12}$$

Taking the logarithm of both sides of Eq. (12) we have

$$Log\left(\frac{\sigma_d - \sigma_s}{\sigma_s}\right) = Log\left[\left(\frac{\dot{\varepsilon}}{C}\right)^{\frac{1}{P}}\right] = \frac{1}{P}Log(\dot{\varepsilon}) - \frac{1}{P}Log(C) \tag{13}$$

Substitution of the known variables obtained from the experimental results ($\dot{\varepsilon}$, σ_d, σ_s), changes the Eq. (13) into the linear Eq. (14)

$$Y_i = aX_i + b \tag{14}$$

In this equation, (a) and (b) coefficients can be obtained from a simple regression of Y_i versus X_i in a two-dimensional diagram.

$$Y_i = Log\left(\frac{\sigma_y - \sigma_s}{\sigma_s}\right) \tag{15}$$

$$X_i = Log(\dot{\varepsilon}_i) \tag{16}$$

Table 2 Parameters of the Cowper-Symonds constitutive model from UCS test

σ_s	σ_d	$\dot{\varepsilon}_i$	X_i	Y_i
3.43	3.51	0.001	-3	-1.6322
	3.68	0.005	-2.30	-1.13735
	3.89	0.01	-2	-0.87254
	4.43	0.1	-1	-0.53529

Table 3 Parameters of the Cowper-Symonds constitutive model from SHPB test

σ_s	σ_d	$\dot{\varepsilon}_i$	X_i	Y_i
3.43	14.13	19	1.28	0.53
	17.67	31	1.49	0.65
	18.76	51	1.73	0.69
	19.94	77	1.88	0.72
	22.28	98	1.99	0.77
	24.11	107	2.03	0.81

The parameter (a) is equivalent to the inverse of (P) as in Eq. (17)

$$a = \frac{1}{P} \tag{17}$$

Substituting the parameters (P) and (b) in Eq. (18), constant (C) would be obtained

$$b = -\frac{1}{P} Log(C) \tag{18}$$

For a given elastic-plastic material, when such an empirically obtained curve matches closely with experimental data, the corresponding C and q will be the material constants. The presented methodology is applied to determine the parameters of the Cowper-Symonds material models for plastic concrete from the results of the compression tests. In each case, the represented data showed in Tables 2-4 were obtained by means of the mean strength values of the 6, 5, and 3 different samples, respectively. The experimental results utilizing to predict

Table 4 Parameters of the Cowper-Symonds constitutive model from triaxial test

σ_s	σ_d	$\dot{\varepsilon}_i$	X_i	Y_i	CP (MPa)
3.43	5.03	0.001	-3	-0.73	0.5
	5.63	0.005	-2.30	-0.48	
	5.92	0.01	-2	-0.4	
	6.9	0.1	-1	-0.2	
6.75	7.63	0.001	-3	-0.88	0.75
	8.1	0.005	-2.30	-0.67	
	8.7	0.01	-2	-0.54	
	9.41	0.1	-1	-0.4	
7.47	8.25	0.001	-3	-0.98	1
	9.1	0.005	-2.30	-0.66	
	9.77	0.01	-2	-0.51	
	10.93	0.1	-1	-0.33	
8.91	9.23	0.001	-3	-1.44	1.25
	9.72	0.005	-2.30	-1.04	
	10.26	0.01	-2	-0.82	
	12.54	0.1	-1	-0.39	
10.45	10.95	0.001	-3	-1.32	1.5
	11.41	0.005	-2.30	-1.036	
	12.07	0.01	-2	-0.81	
	13.7	0.1	-1	-0.51	

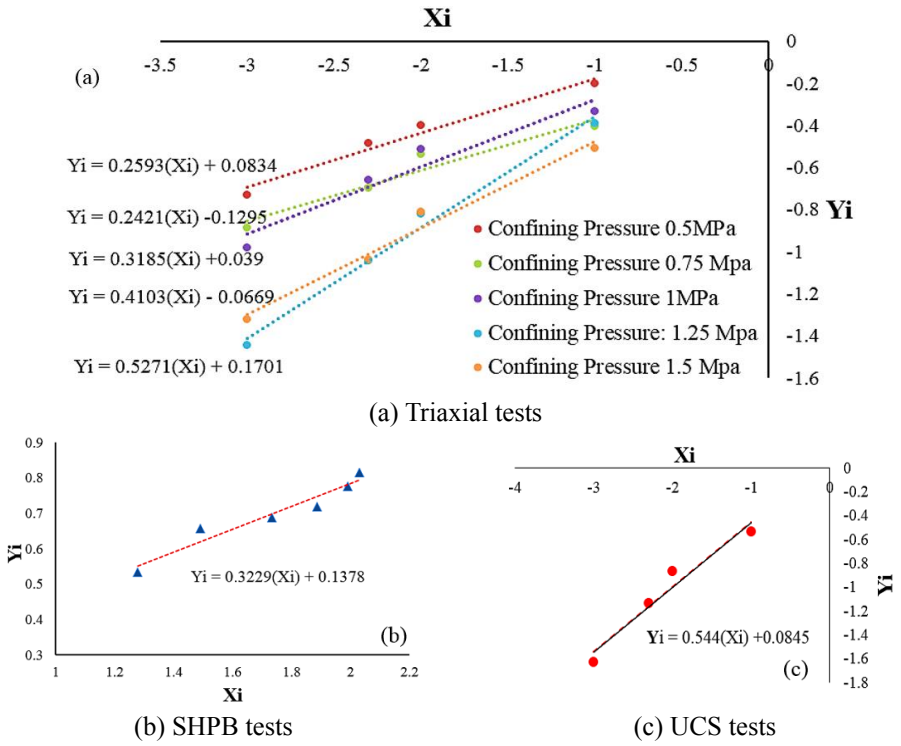

(a) Triaxial tests

(b) SHPB tests (c) UCS tests

Fig. 12 Cowper-Symonds model equations for plastic concrete

Table 5 Cowper-Symonds constitutive equation for plastic concrete in low and intermediate strain rate

Type of experiment	Strain rate range(1/s)	Stress state condition (MPa)	C	q	C-S Equation
UCS	0.0005-0.1	Unconfined	0.699	1.839	$DIF=\left[1+\frac{\dot{\varepsilon}}{0.699}\right]^{1/1.8389}$
SHPB	19-107	Unconfined	0.3744	3.096	$DIF=\left[1+\frac{\dot{\varepsilon}}{0.3744}\right]^{1/3.096}$
		0.5	0.96	3.85	$DIF=\left[1+\frac{\dot{\varepsilon}}{0.96}\right]^{1/3.85}$
		0.75	3.42	4.13	$DIF=\left[1+\frac{\dot{\varepsilon}}{3.42}\right]^{1/4.13}$
Triaxial	0.0005-0.1	1	0.75	3.14	$DIF=\left[1+\frac{\dot{\varepsilon}}{0.75}\right]^{1/3.14}$
		1.25	1.46	2.44	$DIF=\left[1+\frac{\dot{\varepsilon}}{1.46}\right]^{1/2.44}$
		1.5	0.47	1.90	$DIF=\left[1+\frac{\dot{\varepsilon}}{0.47}\right]^{1/1.90}$

the Cowper-Symonds constitutive relationships for plastic concrete.

The graphical representation of Tables 2-4 are shown in Fig. 12. Regression analysis was used to simulate the Cowper-Symonds parameters for all data sets. The parameters to be determined from the experimental results are (C) and (q), to take into account the strain-rate sensitivity. Based on the data summarized in Fig. 12, the mathematical expression for describing the strain-rate effect in the Cowper-Symonds.

Constitutive model is determined. The previously mentioned material parameters and relationships between DIF and the strain-rate are expressed in Table 5. Since the results of the triaxial test are analogous to the natural conditions, are suggested to be used as the input parameters in the numerical models in different depth of the structures.

8. Conclusions

The strain rate effects on the behavior of plastic concrete samples in different stress state condition were investigated. Results of the tests confirm the fact that increasing the strain rate will change the strength of plastic concrete. Therefore, special attention should be paid to the simulation of the structural performance of plastic concrete cut-off wall subjected to dynamic loads.

Within the scope of this research, the following conclusions can be drawn:

1. Analysis of the unconfined laboratory tests, including UCS and SHPB tests, indicates an increase in the concrete strength with increasing the strain rate. However, the results do not follow a linear trend, and all ranges of strain rates should be investigated in two separate domains according to the behavior of the plastic concrete. Concrete strength increases with increasing strain rate, following a logarithmic trend at quasi-static and low strain rates in UCS tests. At intermediate strain rates in SHPB tests, power and exponential trend lines have been proposed.
2. The trend of increasing in DIF versus the log of strain-rate can be divided into weak sensitivity area and strong sensitivity area.
3. In the UCS tests, in low strain rate range (0.0005 to 0.1(1/s)), a slight increase can be observed in concrete compressive strength with increasing the strain rate. The maximum dynamic compressive strength in these ranges is ~1.3 times more than the static strength.
4. In the SHPB tests, in the intermediate strain rate range (19 to107 (1/s)), a shift was observed in the results with a considerable increase in the strength. The DIF factor achieves values of 4.42 to 7.54 in comparison to the static state.
5. In the triaxial tests, increasing the strain rate and the confining pressure applied to the plastic concrete specimens causes a considerable increase in the compressive strength of the plastic concrete. An increase from 28% to 45% was observed in the DIF, when the strain rate and confining pressure were enhanced from 0.0005 to 0.1 (1/s) and 0.5 to 1.5 (MPa), respectively.
6. Cowper-Symonds material models were calibrated based on the experimentally obtained results.

Acknowledgments

The authors wish to thank professor Gholamhosein Majzobi of the impact laboratory, Bu Ali Sina University and Farhad Sheykhani of the rock mechanic laboratory, Tarbiat Modares University, for their help in the experiments. The research was financially supported by the Tarbiat Modares University from the Grant Number 9460522003.

Competing Interests

The authors declare no conflict of interests regarding the

publication of this paper.

References

Al Salahi, A.A. and Othman, R. (2016), "Constitutive equations of yield stress sensitivity to strain rate of metals: A comparative study", *J. Eng.*, Article ID 3279047, 7. http://dx.doi.org/10.1155/2016/3279047.

ASTM (1989), Test Method for Unconfined Compressive of Cohesive Soils, Annual Book of ASTM Standards, American Society of Testing and Materials, Philadelphia, ASTM D2166.

ASTM (1989), Test Method for Unconsolidated Undrained Compressive Strength of Cohesive Soils in Triaxial Compression, Annual Book of ASTM Standards, American Society of Testing and Materials, Philadelphia, ASTM D2850.

Bischoff, P.H. and Perry, S.H. (1991), "Compressive behavior of concrete at high strain rates", *Mater. Struct.*, **24**(144), 425-450. https://doi.org/10.1007/BF02472016.

Brara, A. and Klepaczko, J.R. (2006), "Experimental characterization of concrete in dynamic tension", *Mech. Mater.*, **38**(3), 253-267. https://doi.org/10.1016/j.mechmat.2005.06.004.

Chen, X., Liu, Z., Lu. J. and Fan, X. (2018), "Compressive behavior of concrete under high strain rates after freeze-thaw cycles", *Comput. Concrete*, **21**(2), 209-217. http://dx.doi.org/10.12989/cac.2018.21.2.209.

Chen, X., Wu, S., Zhou, J., Chen, Y. and Qin, A. (2013). "Effect of testing method and strain rate on stress-strain behavior of concrete", *J. Mater. Civil Eng.*, **5**(11), 1752-1761. https://doi.org/10.1061/(ASCE)MT.1943-5533.0000732.

Cusatis, G. (2011), "Strain-rate effects on concrete behavior", *Int. J. Impact Eng.*, **38**(4) 162-170. https://doi.org/10.1016/j.ijimpeng.2010.10.030.

Dharan, C. and Hauser, F. (1970), "Determination of stress-strain characteristics at very high strain rates", *Exp. Mech.*, **10**(9), 370-376. https://doi.org/10.1007/BF02320419.

Gad, E.F., Wilson, J.L., Moore, A.J. and Richards, A.B. (2005), "Effects of mine blasting on residential structures", *J. Perform. Constr. Facil.*, **19**(3), 222-228. https://doi.org/10.1061/(ASCE)0887-3828(2005)19:3(222).

Grote, D.L., Park1, S.W. and Zhou, M. (2001), "Dynamic behavior of concrete at high strain rates and pressures: I. experimental characterization", *Int. J. Impact Eng.*, **25**, 869-886. https://doi.org/10.1016/S0734-743X(01)00020-3.

Guo, Y.B., Gao, G.F., Jing, L. and Shim, V.P.W. (2017), "Response of high-strength concrete to dynamic compressive loading", *Int. J. Impact Eng.*, **108**, 114-135. https://doi.org/10.1016/j.ijimpeng.2017.04.015.

He. Z.J. and Ding. M.J. (2019). "The dynamic mechanic's behavior on triaxial compression of the recycled aggregate concrete", *IOP Conf. Series, Earth. Environ. Sci.*, **283**, 012020. https://doi.org/10.1088/1755-1315/283/1/012020-1.

ICOLD (1985), Filling Materials for Watertight Cut-off Walls, Bulletin No. 51.

Jones, N. (1989), *Structural Impact*, Cambridge University Press.

Kai, M.F., Xiao, Y., Shuai, X.L. and Ye, G. (2016), "Compressive behavior of engineered cementitious composites under high strain-rate loading", *J. Mater. Civil Eng.*, https://doi.org/10.1061/(ASCE)MT.1943-5533.0001781.

Kim, D.J., Sirijaroonchai, K., El- Tawil, S. and Naaman, A.E. (2010), "Numerical simulation of the Split Hopkinson Pressure Bar test technique for concrete under compression", *Int. J. Impact Eng.*, **37**(2), 141-149. https://doi.org/10.1016/j.ijimpeng.2009.06.012.

Krishnappa, N., Bruneau, M. and Warn, G. (2013), "Weak-axis behavior of wide flange columns subjected to blast", *J. Struct. Eng.*, **140**(5), 1-9. https://doi.org/10.1061/(ASCE)ST.1943-541X.0000917.

Li, Y., Qiu, W.C., Ou, Z.C., Duan, Z.P. and Huang, F.L. (2012), "Strain-rate effects on interaction between Mode I matrix crack and inclined elliptic inclusion under dynamic loadings", *Struct. Eng. Mech.*, **44**(6), 801-814. http://dx.doi.org/10.12989/sem.2012.44.6.801.

Lindholm, U.S. (1964), "Some experiments with the split Hopkinson pressure bar", *J. Mech. Phys. Solid.*, **12**, 317-335.

Mahboubi, A. and Ajorloo, A. (2005), "Experimental study of the mechanical behavior of plastic concrete in triaxial compression", *J. Cement Concrete Res.*, **35**(2), 412-419. https://doi.org/10.1016/j.cemconres.2004.09.011.

Marais, S.T., Tait, R.B., Cloete, T.J. and Nurick, G.N. (2004), "Material testing at high strain rate using the split Hopkinson pressure bar", *Lat. Am. J. Solid. Struct.*, **1**, 319-339.

Naderi, M. (2005). "Effects of different constituent materials on the properties of plastic concrete", *Int. J. Civil Eng.*, **3**(1), 10-19.

Nateghi, R., Goshtasbi, G. and Nejati, H.R. (2020). "Coupled effects of confining pressure and loading rate on the mechanical behavior of plastic concrete", *J. Mater. Civil Eng.*, **32**(10), 04020292. https://doi.org/10.1061/(ASCE)MT.1943-5533.0003341.

Ngo, T., Mendis, P., Gupta, A. and Ramsay, J. (2007), "Blast loading and blast effects on structures-an overview", *Electron. J. Struct. Eng.*, **7**(S1), 76-91.

Ngo, T., Mohotti, D. and Remennikov, A. (2015), "Numerical simulations of response of tubular steel beams to close-range explosions", *J. Consttr. Steel Res.*, **105**, 151-163. https://doi.org/10.1016/j.jcsr.2014.11.007.

Pająk, M. (2011), "Dynamic response of SFRC under different strain rates-an overview of test results", *7th International Conference Analytical Models and New Concepts in Concrete and Masonry Structures*, June, Kraków.

Pandey, A.K. (2013), "Flexural ductility of RC beam sections at high strain rates", *Comput. Concrete*, **12**(4), 537-552. http://dx.doi.org/10.12989/cac.2013.12.4.537.

Pashang Pisheh, Y. and Hosseini, M.M. (2012), "Stress-strain behavior of plastic concrete using monotonic triaxial compression test", *J. Cent. South Univ.*, **19**, 1125-1131. http://dx.doi.org/10.1007/s11771-012-1118-y.

Riisgaard, B., Ngo, T., Mendis, P., Georgakis, C.T. and Stang, H. (2007), "Dynamic increase factors for high-performance concrete in compression using split Hopkinson pressure bar", *Fracture Mechanics of Concrete and Concrete Structures*, Italy.

Ritchie, C.B., Gow, M., Packer, J. and Heidarpour, A. (2017), "Influence of elevated strain rate on the mechanical properties of hollow structural sections", *Int. J. Prot. Struct.*, **8**(3), 325-351. https://doi.org/10.1177/20414196177215.

Rukhaiyar, S., Sajwan, G. and Samadhiya, N. K. (2017), "Strength behavior of plain cement concrete subjected to true triaxial compression", Department of Civil Engineering, Indian Institute of Technology Roorkee, Roorkee, Uttarakhand, India.

Sakai, Y., Nakatani, M., Takeuchi, A., Omorai, Y. and Kishi, T. (2016). "Mechanical behavior of cement paste and alterations of hydrates under high-pressure triaxial testing", *J. Adv. Concrete Technol.*, **14**, 1-12. https://doi.org/10.3151/jact.14.1.

Sfer, D., Carlo, I., Gettu, R. and Etse. G. (2002), "Study of the behavior of concrete under triaxial compression", *J. Eng. Mech.*, **128**(20), 156-163. http://dx.doi.org/10.1061/(ASCE)0733-9399(2002)128:2(156).

Sheng, Y., Yu-bin, L. and Yong, C. (2013). "The strain-rate effect of engineering materials and its unified model", *Lat. Am. J. Solid. Struct.*, **10**, 833-844. http://dx.doi.org/10.1590/S1679-78252013000400010.

Tay, Y.S. (2009), "Uniaxial compression tests at various loading rates for reactive powder concrete", *Theor. Appl. Fract. Mech.*, **52**(1), 14-21. https://doi.org/10.1016/j.tafmec.2009.06.001.

WeerheijmJ, J. and Van Doormaal, J. (2007), "Tensile failure of concrete at high loading rates: New test data on strength and fracture energy from instrumented spalling tests", *Int. J. Impact Eng.*, **34**(3), 609-626. https://doi.org/10.1016/j.ijimpeng.2006.01.005.

Yiben, Z., Lingyu, S., Lijun, L., Taikun, W. and Le, S. (2019), "Experimental and numerical investigations on low-velocity impact response of high strength steel/composite hybrid plate", *Int. J. Impact Eng.*, **123**, 1-13. https://doi.org/10.1016/j.ijimpeng.2018.08.015.

Yu, S.S., Bin, L.Y. and Yong, C. (2013), "The strain-rate effect of engineering materials and its unified model", *Lat. Am. J. Solid. Struct.*, **10**(4), 833-844. http://dx.doi.org/10.1590/S1679-78252013000400010.

Zhang, F., Wu, C. and Zhao, X. (2015), "Numerical modeling of concrete-filled double-skin steel square tubular columns under blast loading", *J. Perform. Constr. Facil.*, **29**(5), B4015002. http://dx.doi.org/10.1061/(ASCE)CF.1943-5509.0000749.

Zhang, X.X., Ruiz, G. and Yu, C. (2008). "Experimental study of combined size and strain rate effects on the fracture of reinforced concrete", *J. Mater. Civil Eng.*, **20**(8), 544-551. http://dx.doi.org/10.1061/(ASCE)0899-1561(2008)20:8(544).

Zhao, P. and Lok, T.S. (2005), "Adaptation of impactor for the split Hopkinson pressure bar in characterizing concrete at medium strain rate", *Struct. Eng. Mech.*, **19**(6), 603-618. http://dx.doi.org/10.12989/sem.2005.19.6.603.

HK

Abbreviations

A_0 = cross-sectional area of the bars
a =Particle acceleration
American Society for Testing and Materials (ASTM)
ASTM =American Society for Testing and Materials
B/C =Water/bentonite
e_0 =longitudinal wave speed of the bars
C =A Cowper-Symonds fitting parameter
Cp =P-wave velocity
DIF =Dynamic increase factor
E_0 = Elastic modulus of the input bar or output bar
Eq =Equation
Fig =Figure
ICOLD =International committee of large dams
LVDT =Linear variable differential transformer
PGA =Peak ground acceleration
P- wave =Primary wave
Q =A Cowper-Symonds fitting parameter
S =Second
Split Hopkinson Pressure Bar (SHPB)
T =Time
U =Particle displacement
UCS =unconfined compressive strength
V =Particle velocity
W/C =Water/cement
x =Travelling distance of the wave
σ =Stress
σ_s **=**Peak of uniaxial compression strength (static state of loading)
σ_d =Peak of dynamic uniaxial compression strength
$\dot{\varepsilon}$ =Strain rate
ε =Strain
ε_T =Amplitudes of the transmitted strain pulses
ε_R =Amplitudes of the reflected strain pulses
φ_d **=**Friction angle in dynamic loading
υ =Poisson ratio